ON-LINE IDENTIFICATION OF SENSORY SYSTEMS USING PSEUDORANDOM BINARY NOISE PERTURBATIONS

D. P. O'LEARY *and* V. HONRUBIA

From the Departments of Surgery (Division of Head and Neck) and Anatomy, University of California, Los Angeles, California 90024.
Dr. O'Leary's present address is the Department of Otolaryngology, University of Pittsburgh Eye and Ear Hospital, Pittsburgh, Pennsylvania 15213.

ABSTRACT A technique of on-line identification of linear system characteristics from sensory systems with spike train or analog voltage outputs was developed and applied to the semicircular canal. A pseudorandom binary white noise input was cross-correlated with the system's output to produce estimates of linear system unit impulse responses (UIRs), which were then corrected for response errors of the input transducers. The effects of variability in the system response characteristics and sensitivity were studied by employing the technique with known linear analog circuits. First-order unit afferent responses from the guitarfish horizontal semicircular canal were cross-correlated with white noise rotational acceleration inputs to produce non-parametric UIR models. In addition, the UIRs were fitted by nonlinear regression to truncated exponential series to produce parametric models in the form of low-order linear system equations. The experimental responses to the white noise input were then compared with those predicted from the UIR models by linear convolution, and the differences were expressed as a percent mean-square-error (%MSE). The average difference found from a population of 62 semicircular canal afferents was a relatively low mean and standard deviation of 10.2 ± 5.9 SD %MSE, respectively. This suggests that relatively accurate inferences can be made concerning the physiology of the semicircular canal from the linear characteristics of afferent responses.

INTRODUCTION

White noise inputs have been used recently to characterize sensory systems by cross-correlation analyses in the time domain (Marmarelis and Naka, 1973 *a,b,* 1974). This analysis is based formally on the classical work of Wiener (1958) and Kolmogorov (1941), who developed independently a method for obtaining a characterization of a system as the time domain response of an equivalent linear filter. The discrete form of this characterization was a set of weighting coefficients, spaced at equal times and extending from the present into the negative time domain, that determined the manner in which past inputs were filtered by the system to result in the present output. This characterization was described as a unit-impulse response (UIR) because the time course of the weighting coefficients was identical to that of the trajectory of the sys-

tem's response to an impulse of unit energy but infinitesimal duration. These authors showed further that, whereas unit-impulses were unrealizable as actual inputs, an accurate estimate of the UIR could be obtained in practice by the cross-correlation of input with output provided that the input was a sufficiently good approximation to white noise; the latter was defined as having a constant power spectral density over a frequency band wider than that of the system, or equivalently, an autocorrelation function that was itself a unit impulse in the time domain. This approach has certain advantages for obtaining accurate characterizations from sensory data. (*a*) Sensory outputs, such as receptor potentials or spike trains, have stochastic (random) components, deriving from both internal and external sources, that are unrelated to the experimental inputs. The UIR as derived by input-output cross-correlation analysis is not corrupted by either internal or external noise sources as long as the latter are uncorrelated with the input noise. (*b*) A white noise input can be considered the equivalent of a superposition of sinusoids of all frequencies in a band that is wider than that of the system. The system's response across its entire spectral range can thus be determined from a relatively brief experimental protocol performed under relatively stationary experimental conditions. The use of white noise inputs allows quantitative estimations of both time and frequency domain linear characteristics and also nonlinear characteristics to be obtained from a properly designed analysis.

The nonlinear techniques utilizing white noise inputs were reviewed by Marmarelis and Naka (1973 *a,b*) who applied them to determine characterizations in the form of integral equations of the catfish retinal ganglion and bipolar cell responses to Gaussian white noise inputs of both light and electrical current. Although elegant both theoretically and in the retinal applications cited above, the nonlinear Wiener analysis has the practical disadvantage that extensive computer computations are required to produce the integral equations; and furthermore, the results are generally not available for evaluation until after the experiment is terminated. This is due in large part to the use of Gaussian inputs which, even when presented periodically, have a large number of possible states in the input space. An alternative to the use of Gaussian inputs is to employ digital noise sources in the form of step sequences that can be generated and implemented with laboratory computers for on-line use. For example, sequences of binary input states that satisfy certain criteria were shown to be an excellent approximation to band-limited white noise for use in systems' identification analysis (Birdsall and Ristenbatt, 1958; Briggs et al., 1965; Davies, 1970). Although used widely in the design of automated controllers for industrial processes, digital noise sources have not been exploited previously for on-line modeling of sensory systems. An advantage of on-line characterization is that the protocol can be varied, or even controlled automatically, under the command of programmed decision criteria, in order to best use the computed results to further refine the experimental protocol with the same preparation.

This report will describe a technique of on-line systems modeling of sensory input-output data that employs pseudorandom binary sequences as test inputs. The focus of this report is the expediency of obtaining rapid and accurate unit impulse response

representations that are corrected appropriately for the non-ideal white noise characteristics of the input signals. However, this technique retains the advantages of white noise inputs for determining frequency domain descriptions such as gain, phase and coherence by employing computations based on the fast fourier transform (Cooley and Tukey, 1965; Otnes and Enochson, 1972), and, moreover, the input-output data can be used also for a subsequent off-line nonlinear analyses. Our objective in developing this approach was to characterize rapidly a large population of unit afferent responses from nerves innervating the semicircular canal and to correlate the response characteristics with the anatomical innervation patterns (O'Leary, et al., 1974). This receptor has been characterized accurately in previous studies by deriving low-order linear transfer functions from the responses to deterministic inputs (sinusoids, steps or ramps) from an off-line analysis (Groen et al., 1952; Fernandez and Goldberg, 1971; Precht et al., 1971; Milsum and Jones, 1969); whereas the present report describes the alternative of employing white noise inputs to obtain accurate on-line linear representations. It is essential that the major characteristics of this technique are illustrated first with known linear systems and results from testing a linear filter circuit with known parameters will be described. The results of an analysis of afferent responses from the semicircular canal will be presented in a way that illustrates those technical aspects that are relevant to applications of this approach to biological systems in general with either spike train or analog voltage outputs.

THEORY

A system that exhibits a linear functional relation between the output $y(t)$ and the input $x(t)$ can be characterized as a filter in the time domain by the linear convolution integral

$$y(t) = \int_0^\infty h(\tau)x(t - \tau)\,d\tau, \tag{1}$$

where $y(t)$ is the output at the time t, $x(t - \tau)$ is the input that occurred at a time $(t - \tau)$ in the past, and $h(\tau)$ is a weighting function which is multiplied by the past inputs and thus determines their relative influence on the present output. The function $h(\tau)$ thus characterizes the system by the way in which past inputs are weighted to influence the present output, and it is formally identical to the first-order or linear kernel described in nonlinear Wiener (1958) theory. As derived classically, $h(\tau)$ was described as a UIR determinable from experimental responses to white noise inputs by the use of a cross-correlation analysis as described in Appendix A.

The Generation and White Noise Properties of Pseudorandom Binary Sequences (PRBS)

A type of pseudorandom white noise developed recently is a repeating sequence of N binary input states, e.g. (0, 1) or $(+a, -a)$. The properties of these sequences were described for, and they have been used primarily in, applications in process control

(Briggs et al., 1965; Davies, 1970). Maximal length sequences with the necessary properties are generated by a shift register with an appropriate digital feedback network as shown in Fig. 1 *a*. Alternatively, a digital computer program can duplicate the same algorithm to produce a sequence, e.g. Fig. 1 *b*, which is then converted to a binary stimulus by the use of appropriate relay control circuitry. Algorithms for generating various sequences have been described in detail (e.g., Briggs et al., 1965; Davies, 1970). Properties that are relevant to this study are summarized below:

(*a*) An n-stage shift register generator will produce a maximum length of $N = 2^n - 1$ binary states in each period. If each state is maintained for a time interval Δt before the register is shifted by the next clock pulse, the total period of the sequence is $T = N\Delta t$.

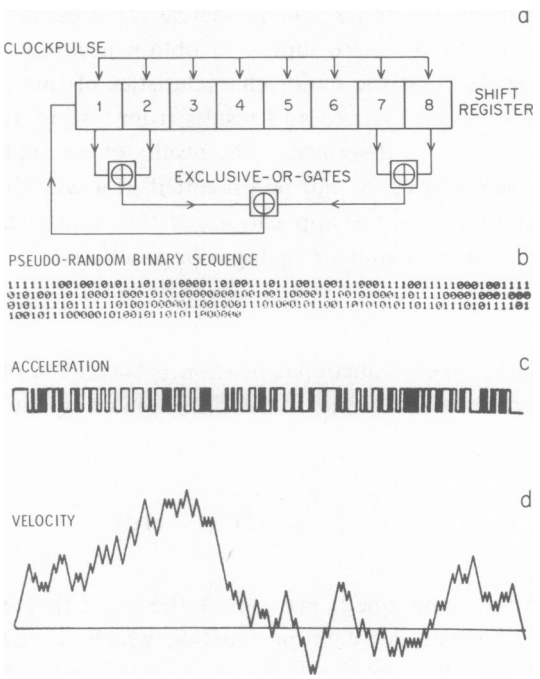

FIGURE 1 The generation and interfacing of a pseudorandom binary sequence (PRBS) noise stimulus. (*a*) A shift register formed from eight flip-flops (FFs) is shown with the output of selected FF pairs fed back through exclusive-or-gates to the first FF stage. A maximum length sequence of $2^8 - 1 = 225$ binary states is generated and repeats periodically as the register is shifted serially by a regularly timed clockpulse. The PRBS can be sampled at the output of any FF and used to control the state of a relay for interfacing with the stimulus-generating apparatus. (*b*) One PRBS period of 255 states as generated either from the circuit in *a* or an equivalent computer algorithm. The sequence repeats in closed circular form after completion of each period. (*c*) Output of a relay controller driven by the PRBS shown in *b*. An up state, corresponding to a 1 in the PRBS, controlled a rotational acceleration stimulus magnitude of $+a$; a down state, corresponding to a 0 in the PRBS, controlled a rotational acceleration magnitude of $-a$. (*d*) Rotational velocity profile of the stimulus as obtained by integration of the acceleration pattern in *c*.

(*b*) If the states have amplitudes $\pm a$, the autocorrelation function (ACF) (as computed from Eq. 27 in Appendix A) is periodic with values

$$\phi_{xx}(\tau) = \begin{cases} a^2[1 - (|\tau|/\Delta t)([N+1]/N)], & 0 \leq |\tau| < \Delta t \\ -a^2/N, & \Delta t \leq |\tau| < T - \Delta t \end{cases} \tag{2}$$

i.e., triangular pulses of height a^2 and base widths $2\Delta t$ which occur at integral multiples of T. There is a negative offset at all other values of T as shown schematically in Fig. 2*a*. For sequences with large N, the negative offset is approximately zero and the triangular pulses at multiples of T are approximations of δ-function impulses that are characteristic for the ACF of a white noise signal as described in Appendix A. This

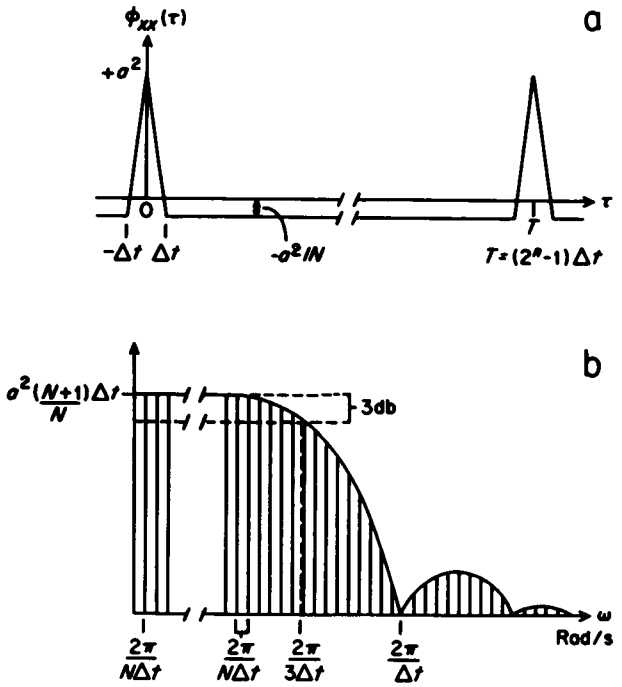

FIGURE 2 Autocorrelation and power spectral density of a pseudorandom binary sequence (PRBS) test stimulus. (*a*) The autocorrelation function (ACF) of a PRBS is shown as a periodic series of triangular pulses separated by regions of negative offset of magnitude $-a^2/N$. The notation used is: a, magnitude of the binary stimulus; Δt, time interval between clock pulses; n, the number of flip-flop stages in the PRBS generator; $N = 2^n - 1$, the number of binary states in one PRBS period; $T = N\Delta t$, the time period of the PRBS. As N becomes large the offset becomes small and the PRBS ACF approximates a periodic series of δ-functions which is the characteristic pattern for the ACF of a periodic white noise source. (*b*) The power spectral density of a PRBS is shown as a line spectrum with line separation = $1/N\Delta t$ Hz. The spectrum has a shape that is characteristic of the function $(\sin x/x)^2$, with the first zero occurring at the clockpulse frequency $1/\Delta t$ Hz, and a constant magnitude $a^2(N+1)\Delta t/N$ which decreases by 3 dB at a frequency of $1/3\Delta t$ Hz. The high- and low-frequency cutoffs of the noise band can be controlled accurately by adjusting Δt and N, respectively.

implies that a close approximation to white noise can be maintained for N sufficiently large.

(*c*) The cross-correlation function (CCF) $\phi_{xy}(\tau)$ is related to the system's UIR $h(\tau)$ by

$$\phi_{xy}(\tau) = \begin{cases} [a^2(N+1)\Delta t/N]h(\tau) - \text{const}, & \tau \geq \Delta t \\ [a^2(N+1)/N]\left[\frac{\Delta t}{2} + \tau\left(1 - \frac{\tau}{2\Delta t}\right)\right]h(\tau) - \text{const}, & 0 < \tau < \Delta t \\ [a^2(N+1)\Delta t/2N]h(0) - \text{const}, & \tau = 0 \end{cases} \tag{3}$$

provided that the period T of the pseudorandom binary sequence (PRBS) is greater than the settling time (or "memory") of the system and that $h(x)$ does not vary significantly from a value $h(\tau)$ over the time interval $(\tau - \Delta t) \leq x \leq (\tau + \Delta t)$.

(*d*) The power-density spectrum of a PRBS, as determined by a substitution of Eq. 2 into the Wiener-Khinchine relationship of Eq. 24 is

$$\Phi_{xx}(\omega) = \frac{a^2(N+1)\Delta t}{N} \sum_{r=1}^{N} \left[\frac{\sin(r\pi/N)}{(r\pi/N)}\right]^2 \delta\left(\omega - \frac{r_2\pi}{N\Delta t}\right) \tag{4}$$

This line spectrum (periodogram) has a constant value of $a^2(N+1)\Delta t/N$ at low frequencies, falls by 3 dB at a frequency given by $[\sin(r\pi/N)/r\pi/N]^2 = 0.707$ or approximately $r = N/3$, and reaches the first zero at a frequency of $1/\Delta t$ Hz as shown schematically in Fig. 2*b*. (The $[(\sin x)/x]^2$ form of Eq. 4 is thus similar to that of the transform of a triangular smoothing window used often with Fast Fourier Transformed data to attenuate the side lobes in the stop band (Gold and Rader, 1969). The frequency band over which the PRBS can be considered band-limited white noise with a constant power spectral density is therefore

$$1/N\Delta t < f < 1/3\Delta t, \tag{5}$$

where the frequency f is in hertz, N is the number of binary states and Δt is the clock pulse period. In practice, Eq. 5 can be used to determine the appropriate parameters for a noise source which spans the desired bandwidth: the clock pulse period Δt is first chosen to correspond to the required high frequency (3 dB) cutoff, and the necessary sequence length N is then determined by the required lower band limit of the noise source. Furthermore, if the PRBS is generated on-line, the bandwidth of the noise source can be changed during an experiment by a programmed selection of appropriate values of N and Δt.

Cross-Correlation of a Spike Train Output with a PRBS Input

The PRBS input $x(t)$ has a constant amplitude over each individual state duration and is switched in amplitude only at discrete times determined by the onset of a new clock-

pulse (Fig. 1 *a*). Eq. 31 for the CCF can therefore be written in the form

$$\phi_{xy}(\tau) = \frac{1}{N\Delta t} \sum_{k=0}^{N-1} x(\tau) \int_{k\Delta t}^{(k+1)\Delta t} y(t + \tau)\, dt, \tag{6}$$

where T is replaced by $N\Delta t$. If the spike train output $y(t + \tau)$ can be approximated as a constant firing rate $\bar{y}$ (i.e. varies negligibly) over the time interval Δt, the integral in Eq. 6 can be approximated as

$$\int_{k\Delta t}^{(k+1)\Delta t} \bar{y}(t + \tau)\, dt \cong \bar{y}_k \Delta t, \tag{7}$$

where $\bar{y}_k$ is the mean firing rate over the kth interval Δt. (For a sufficiently short Δt corresponding, by Eq. 5, to a correct choice of high-frequency noise cutoff to be considered band-limited white noise for the sensory system, the rectangular approximation of Eq. 7 will be relatively accurate.) By substitution of Eq. 7, Eq. 6 becomes

$$\begin{aligned} \phi_{xy}(\tau) &= \frac{1}{N\Delta t} \sum_{j=0}^{N-1} x_j \overline{y_{j+\tau}} \Delta t \\ &= \frac{1}{N} \sum_{j=0}^{N-1} x_j \overline{y_{j+\tau}}. \end{aligned} \tag{8}$$

If the input x_j is binary with amplitudes $\pm a$, Eq. 8 simplifies to

$$\begin{aligned} \phi_{xy}(\tau) &= \frac{a}{N} \left[\sum_{j+} \bar{y}_{j+\tau} - \sum_{j-} \bar{y}_{j+\tau} \right] \\ &= \frac{a}{N} (y_{+a} - y_{-a}) \end{aligned} \tag{9}$$

where the notation

$$y_{+a} = \sum_{j+} \bar{y}_{j+\tau} \tag{10}$$

indicates the summation of output mean rates over *only* those input states that correspond to $+a$, and y_{-a} indicates a similar summation over states corresponding *only* to $-a$. Finally,

$$\phi_{xy}(\tau) = (a/N)\Delta y_\tau, \tag{11}$$

where Δy_τ is defined as $(y_{+a} - y_{-a})$. Eq. 11 shows that, aside from a scale factor a/N, discrete points of the cross-correlation function can be estimated at regularly spaced

times $k\Delta t$, $0 \leq k \leq N - 1$, by simply adding, subtracting, and gating the output because of the binary nature of the PRBS input. Furthermore, the term Δy_τ can be computed as the net number of spikes per period that occurred during $+a$ states minus those that occurred during $-a$ states for a specified relative shift τ between input and output.

Cross-Correlation of an Analog Voltage Output with a PRBS Input

Because experimental outputs can be obtained from certain sensory systems as analog voltages which measure receptor or generator potentials, it is important to include the use of analog outputs in the above analysis. This is done simply by interpreting $\bar{y}_k$ in Eq. 7 as the mean analog voltage amplitude as averaged over the kth state duration. In practice, this is estimated by performing an analog-to-digital conversion of m samples of the output waveform, where the samples are spaced at intervals $\Delta t/m$, and then computing the mean corresponding to each of the PRBS input states. For maximum accuracy, anti-aliasing filters should be employed during digitizing of the analog waveform (Otnes and Enochsen, 1972).

Theoretical Magnitudes of Discrete Time Estimates of the Unit Impulse Response (UIR) $h(\tau)$ for a Sensory Output and a PRBS Input

From Eq. 3, the impulse response $h(\tau)$ is linearly proportional to the cross-correlation $\phi_{xy}(\tau)$ according to

$$h(\tau) = \begin{cases} [N/a^2(N+1)\Delta t]\phi_{xy}(\tau), & \tau \geq \Delta t \\ [2N/a^2(N+1)\Delta t]\phi_{xy}(\tau), & \tau = 0 \end{cases} \tag{12}$$

where the constant term on the right side of Eq. 3 is assumed to be removed by subtracting it from the experimental cross-correlation results, and τ can assume only the discrete values $k\Delta t$, $0 \leq k \leq N - 1$. Then by a substitution of Eq. 11 into Eq. 12,

$$h(\tau) = \begin{cases} \Delta y_\tau/a(N+1)\Delta t, & \tau \geq \Delta t \\ 2\Delta y_\tau/a(N+1)\Delta t, & \tau = 0 \end{cases} \tag{13}$$

is the exact expression for discrete time estimates of the impulse response of a system with a sensory output and PRBS input. The units of $h(\tau)$ are therefore determined by the input and output units: e.g., for a spike train output and Δt expressed in units of seconds, $h(\tau)$ has units of impulses per second divided by those of the input.

METHODS

Isolated labyrinths of the elasmobranch *Rhinobatos productus* (guitarfish) were prepared by removal of the cranium after pithing the brain. A small opening was made in the cartilage overlying the horizontal semicircular canal nerve at the rear of the orbit. The preparation was mounted at the center of a Goerz/Inland (Pittsburgh, Pa.) Rate-of-Motion Table (Model

800) with the plane of the horizontal semicircular canal parallel to the plane of rotation. The horizontal canal nerve of this species branches into separate bundles, each containing from 30 to 500 individual cells, which lie over the utricle. The technique used to obtain single afferent response recordings was similar to that used by Groen et al. (1952) in *Raja clavata* (O'Leary et al., 1974). Fine filaments, each containing from 10 to 30 dendrites, were isolated from a bundle by squeezing portions with a fine forceps at a region distal to the receptor, severing the fibers from the bundle and then pulling the filament toward the receptor to result in a sub-bundle 5–12 mm in length. This was suspended in air by attaching the end to the tip of a sharpened stainless steel forceps which served as the active electrode. Single unit neural activity was recorded differentially from the filament, amplified conventionally and broadcast to a receiver via frequency modulation telemetry. The spike trains were led simultaneously to conventional display and recording apparatus and also to a PDP-11 computer system for on-line cross-correlation with the PRBS noise input.

Generation of PRBS Noise Inputs

Band-limited white noise in the form of PRBS was generated by a PDP-11 computer program which duplicated the algorithm shown in Fig. 1 *a*. The 0 and 1 states of the PRBS were converted to signals of 0 and +5 V, respectively, which controlled the binary states of a relay. The relay states, shown in Fig. 1 *c*, determined the direction (clockwise or counterclockwise) of rotational acceleration of the rotating table. The resulting acceleration of the table was of a constant magnitude of $100°/s^2$ but pseudorandom direction as determined by the PRBS. One period of the table velocity trajectory is shown schematically in Fig. 1 *d* as the first integration of the acceleration sequence of Fig. 1 *c*. The errors in impulse response estimates resulting from the finite switching times of the table due to inertia were corrected by the input-transducer error analysis described below and in Appendix B.

Cross-Correlation and Impulse Response Computations

The cross-correlations were computed initially off-line by digitizing a spike train recorded on analog tape that corresponded to an integral number of periods of the PRBS. The PRBS, recorded on a second tape channel, was used to recalibrate the individual state durations and also to synchronize the spike train output with the input, for use during the cross-correlation computation. The mean firing rate over each state interval, shown as $\bar{y}_k$ in Eq. 7, was computed by counting the number of impulses that occurred during that interval for all states in one period. These values were then summed with the corresponding counts from other periods to result in a period histogram of impulses per state as averaged over 6–20 PRBS periods. The resulting averaged output trajectory (in units of impulses per state) was cross-correlated with the PRBS input by the gating, adding and subtracting computation described in the Theory section. The PRBS parameters used were: $N = 255$, $\Delta t = 92.0$ ms and $p = 6$–20 to correspond to band-limited white noise (as determined by Eq. 5) from 0.04 to 4 Hz. The constant base-line offset shown in Eq. 3 was removed after the cross-correlation by subtracting the mean of the last 32 points from all of the points. The cross-correlation was scaled by the factors shown in Eqs. 12 and 13, and the necessary input transducer correction factors described in Appendix B were included in the displayed impulse responses.

In later experiments, the above analysis was performed on-line by a single assembly language program that generated the PRBS stimulus, digitized the spike train, computed the cross-correlation and displayed the impulse response estimates. The on-line impulse response estimates were monitored as they were computed by a computer display of the contents of a data storage array. Because cells with poor sensitivities required more periods of the PRBS to result in an acceptable signal-to-noise ratio of the impulse response than that required by more

sensitive units, the on-line display was used as a visual criterion for determining the necessary number of PRBS periods that resulted in adequate resolution of the impulse response for each unit.

Determination of Input-Transducer Error for the Servocontrolled Rotational Stimulus

The analysis described in the Theory section is exact only for the ideal case that the PRBS approximates wide-band white noise and that the input transducer system maintains the white-noise properties by switching in negligible time between the binary states. These conditions are never fulfilled exactly because the PRBS has inherent finite bandwidth limitations and electromechanical systems used as practical stimulus inputs have finite switching times determined by their individual response characteristics. Godfrey and Murgatroyd (1965) analyzed the effects of both the PRBS finite-bandwidth limitations and the finite switching times of input transducers and derived theoretically the corrections that must be applied in the UIR discrete estimates as a function of the magnitudes of these effects. A summary of their theoretical derivations which apply to the corrections necessary for the rate table's error is described in Appendix B. The transducer error for the Inland Controls Model 800 rate-of-motion table used to deliver a rotational acceleration stimulus was estimated by monitoring the acceleration profile of the system in response to a PRBS input of $a = \pm 100°/s^2$, $\Delta t = 92.0$ ms and $N = 255$. Fig. 3 *a* shows a superposition of 10 oscillographic sweeps of the table acceleration with the CRO sweep triggered by a positive-going transition of the PRBS. The system was underdamped which resulted in overshoot and ringing at the resonant frequency of 55 Hz; however, the small amplitude of this oscillation contributed negligible power to either the system or the PRBS noise band which had a 3 dB upper frequency cutoff of < 5 Hz. The transitions between binary acceleration states were fitted approximately by average slopes of a

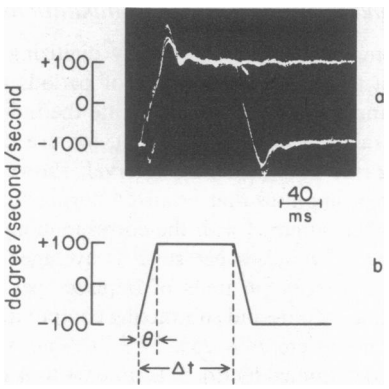

FIGURE 3 Input-transducer error of a Goerz/Inland model 800 rate-of-motion table to a PRBS angular acceleration input with state duration $\Delta t = 0.092$ s. (*a*) 10 transitions of $\pm a = 100°/s^2$ are shown superimposed on an oscilloscope with the sweep triggered on the − to + transition. Two different trajectories occurred during the transitions because of the difference in inertial response of the table when it was commanded to change rotational direction as opposed to merely changing the direction of acceleration. (*b*) Average trapezoidal response as fitted to *a* by assuming symmetrical positive and negative trapezoidal transition slopes. The transition time was $\theta = 18.5$ ms for a $\Delta t = 92.0$ ms resulting in a transducer input error of approximately $\theta = \Delta t/5$. The overshoot and ringing shown in the figure occurred at the rate table's resonance of 55 Hz, which was not within the physiological system's bandwidth.

symmetrical trapezoid as shown in Fig. 3*b*. This trapezoid represents a transducer input error of $\theta = 92/18.5$, or approximately $\Delta t/5$.

By substitution of this value into Eq. 39 and assuming a system with a fastest transient given by $h(\tau) = ke^{-b\tau}$, where k and b are constants, the percentage errors resulting from *both* the band-limited PRBS and the rotating table are

$$\text{Error}/100\% = \begin{cases} -0.247 + 0.114(b\Delta t) - \frac{1}{3}(b\Delta t), & \tau = 0 \\ -0.010 + 0.123(b\Delta t) + \frac{1}{12}(b\Delta t)^2, & \tau = \Delta t \\ 0.133(b\Delta t) + \frac{1}{12}(b\Delta t)^2, & \tau \geq \Delta t + \theta \end{cases} \quad (14)$$

where the last terms on the right-hand side are the error contributions from bandlimiting of the PRBS. Corrections for $h(\tau)$ were computed by determining an approximate value of b for each UIR by a nonlinear regression program, subtracting the results of Eq. 14 from one and multiplying $h(\tau)$ by the results.

Computation of Exponential Series Representations of Impulse Response Estimates

Quantitative linear systems representations were obtained from the impulse response estimates by computing the best-fit coefficients c_i and p_i in the equation

$$h(\tau) = \sum_{i=1}^{m} c_i e^{p_i \tau} \quad (15)$$

by a nonlinear least-squares FORTRAN program, BMD07R, that computed a stepwise Gauss-Newton iteration for a user-specified nonlinear function (Dixon, 1973). As written originally, this program requires large memory computers; however, it was modified minimally in order to run on a 16k PDP-11 computer. The order m of the fit for each data file was determined as the lowest order that produced a sharp decrease in the residual sum of squares.

RESULTS

Test of the PRBS Identification Technique with Known Linear Circuits

The circuit shown schematically in Fig. 4*a* was used to determine the resolution and sources of error of this technique with known linear elements. A low-pass resistance-capacitance (RC) filter (Fig. 4*b*) was connected in the box labeled $h(\tau)$ in Fig. 4*a* and driven by a PRBS signal of ±2.5 V. The filter responded to voltage inputs with analog outputs, at terminal A, that were analogous to certain types of nonadapting receptor potentials (Fourtes, 1971). A second output, P, was a pulse train with a carrier rate modulated by the voltage at A; this output type is analogous to regularly-timed first-order tonic afferents found in the vestibular system. The carrier rate was determined by setting the magnitude of an adjustable positive dc bias on the input. Increasingly positive voltage at A resulted in increased pulse frequency at P, analogous to that described as resulting from receptor depolarization, whereas increasingly negative voltages resulted in decreased pulse frequencies analogous to the effects of hyperpolarization as described for certain receptors such as the lateral line (e.g., Flock, 1971). Although the

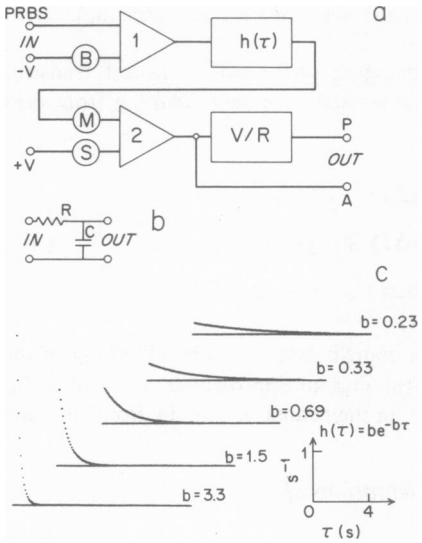

FIGURE 4

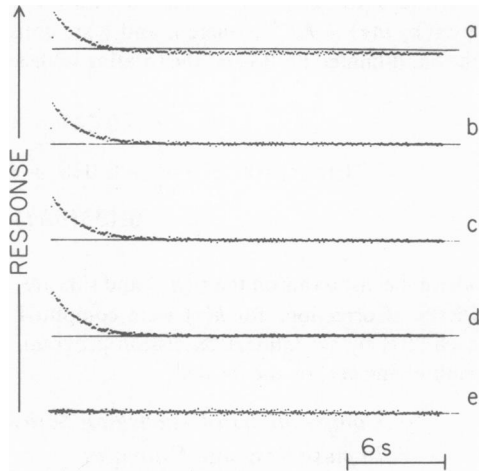

FIGURE 5

FIGURE 4 (*a*) A schematic illustration of an analog linear circuit used for simulating receptor potential and spike train responses to pseudorandom binary sequence (PRBS) inputs. Linear circuits were connected as systems to be identified in the "black box" labeled $h(\tau)$. Amplifier 1 summed a PRBS of magnitudes 0 and 5 V and a biased voltage divider B to result in a symmetric stimulus of magnitude ±2.5 V. Amplifier 2 summed a fraction of the system's analog voltage output, as adjusted by voltage divider M, and a positive offset bias as adjusted by voltage divider S. This sum was the input to a linear voltage-to-rate converter (V/R) which converted the offset analog voltage to modulations in rate of a regularly timed train of 1 ms duration pulses centered at a carrier rate. The output P resembled the spike train output of a tonic, regularly firing sensory afferent that responded to stimuli with symmetric modulation centered at a spontaneous rate. The analog voltage output A resembled certain nonadapting receptor potentials that can occur in response to input stimuli. Both the spontaneous pulse rate and modulation depth were variable and controlled by voltage dividers S and M, respectively. S was first set to result in a desired spontaneous rate R_o at the output P and a corresponding analog voltage offset A_o at the output with the PRBS input grounded. An input of +2.5 V was then applied at the PRBS input and M was adjusted to result in outputs of $2A_o$ at A and $2R_o$ at P; this was defined as a dc modulation depth of 100%. Modulation depths of m times 100% were determined and defined similarly to result in outputs of mA_o and mR_o at A and P, respectively. Additional amplifiers (not shown) were used to insure proper impedance matching and amplitude scaling. (*b*) Linear low-pass filter circuit with adjustable values of resistance R and capacitance C used as the test system in *a*. (*c*) Theoretical impulse response functions $h(\tau) = b \exp(-b\tau)$ of the circuit in *b* with five different reciprocal time constants $b = 1/RC$.

FIGURE 5 Illustration of the computation of $h(\tau)$ for the linear low-pass resistance-capacitance filter circuit of Fig. 5 *b* with a pulse train output modulated by a PRBS input signal with a simulated transducer error of $\theta = \Delta t/5$. Ordinate: response in arbitrary units; abscissa: time. The filter time constant was $b = 0.69\ s^{-1}$. (*a*) The cross-correlation estimate $\phi_{xy}(\tau)$ is shown after computation by cross-correlation of four periods of the pulse modulated response with the PRBS input using Eq. 9. The negatively offset baseline corresponds to the constant term in Eq. 3. (*b*) $\phi_{xy}(\tau)$ after correction for the offset base line by substraction of the mean of the last 32 points from all values. (*c*) Impulse response estimate $h(\tau)$ as determined by multiplying $\phi_{xy}(\tau)$ by the coefficients in Eq. 13; the magnitude of $h(0)$ was doubled as required by Eq. 13. (*d*) $h(\tau)$ after correction for the PRBS bandwidth limitation and the simulated transducer error of $\theta = \Delta t/5$; the correction factors as computed from Eq. 18 were $1.26\,h(0)$, $1.00\,h(\Delta t)$, and $0.99\,h(k\Delta t)$, $1 < k \leq 255$. (*e*) A control for zero correlation as obtained by cross-correlation of the PRBS with four periods of unmodulated (i.e. "spontaneous") pulse train output.

circuit of Fig. 4*a* could have been simulated entirely by a digital computer program for test purposes, we chose to build it from hardware circuit modules in order to test directly the unaltered analysis programs used for experimental physiological data. In Fig. 4*c* are shown theoretical impulse responses, generated and plotted by a computer program, corresponding to those of the filter in Fig. 4*b* with equation $h(\tau) = b\exp(-b\tau)$, where $b = 1/RC$, for the five values of b indicated in the figure. Only discrete points that are separated by time intervals of 92 ms are shown in Fig. 4*c* for purposes of comparison with experimental results to be described.

In order to include the effects of transducer input errors in the analysis, the PRBS voltage inputs were first converted to constant slope transitions, with the characteristics shown in Fig. 3*b* by use of a variable slope circuit (Ling Model 100, Ling Electronic Div., Altec Corp., Anaheim, Calif.). In effect, this input simulated the approximate transducer error of $\theta = \Delta t/5$ of the rate-of-motion table used in the physiological experiments. The resulting waveform was a sequence of trapezoids with pseudorandom durations and constant, symmetric slopes. It was applied as the input to the circuit of Fig. 4*a,b*, with time constant $b = 0.69\ s^{-1}$ and a dc modulation depth of 300% (described in Fig. 4 legend). Fig. 5 illustrates the results of the procedure used to obtain $h(\tau)$ as computed in the following order: cross-correlation (*a*), removal of offset base line (*b*), conversion to impulse response (*c*), and application of correction factors (*d*) for the simulated input transducer error. The result shown in Fig. 5*d* agrees favorably with the theoretical curve for $b = 0.69\ s^{-1}$ shown in Fig. 4*c* except for small fluctuations in the points. These fluctuations could be minimized by conventional data smoothing procedures; however, no digital smoothing other than that resulting from averaging the cross-correlations from four periods was used in order to better illustrate the technical characteristics. Fig. 5*e* shows the result of an identical computation but from a segment of unmodulated ("spontaneous") pulse train output. The results do not exhibit response amplitudes that are significantly correlated with the PRBS; therefore, the point fluctuations shown are largely a result of autocorrelated "noise" in the technique as described below. The necessary corrections for input transducer errors were less than 1% for all except the first point at $h(0)$ which required an amplitude correction of +26%. As described in Methods, however, these corrections are a function of the value of b in Eq. 14, and, for a given value of Δt, become greater as b increases. But when Δt is sufficiently short such that the finite-amplitude portion of $h(\tau)$ spans at least $1/5$ of the PRBS period, the results of Fig. 5*d* show that the effects of transducer input errors are negligible (within overall experimental error) for all points except that at $h(0)$. This suggests that optimal accuracy could be attained by viewing $h(\tau)$ estimates computed on-line and varying Δt until the above criterion is satisfied.

The procedure summarized in Fig. 5 was used to obtain $h(\tau)$ estimates for all subsequent results. Two protocols were used with the circuit of Fig. 4*a,b:* (*i*) a fixed time constant $b = 1/RC$ with variable modulation depths (Figs. 6, 7), and (*ii*) a fixed modulation depth with variable time constants (Figs. 8, 9).

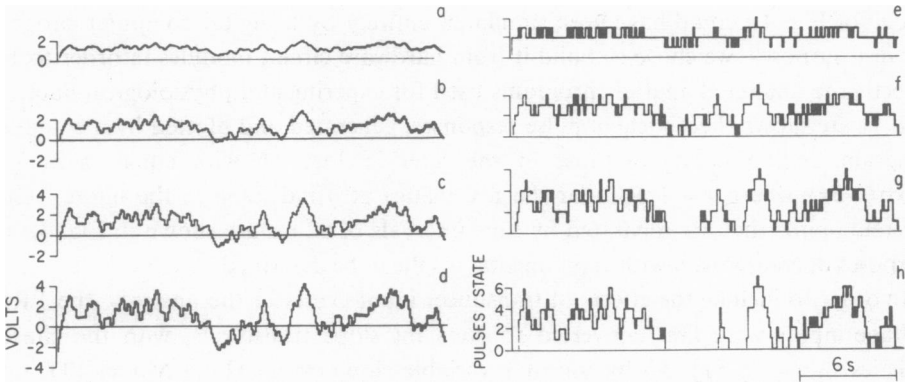

FIGURE 6 Experimental responses of the linear filter circuit of Fig. 5 with $b = 1.5\ s^{-1}$ to a single period of the PRBS input of Fig. 1 with $\Delta t = 92.0$ ms. Left column: analog voltage outputs at *A* of Fig. 5. The voltage divider *M* in Fig. 5 was adjusted to produce four different modulation levels: *a* 100%, *b* 200%, *c* 300%, and *d* 400%. Each histogram bin magnitude is the voltage averaged over a state duration Δt. The response contours resemble approximately that of the integrated velocity profile of Fig. 1 *d* because of the low-pass filter approximation to an integrator. Right column: pulse interval modulator outputs at *P* of Fig. 5 corresponding to the analog voltages in the left column. Ordinate: number of pulses that occurred during each state Δt; abscissa: time in bin units of $\Delta t = 92.0$ ms. The circuit voltage divider *S* was adjusted so that 1 V at *A*, Fig. 5, resulted in an unmodulated carrier rate of 40 pulses/s at *P*, Fig. 5. This carrier was modulated only for positive analog voltages. The periods with zero pulses correspond to negative analog voltages, and are analogous to "silent periods" observable in sensitive sensory afferents in response to inhibitory stimuli. These silent periods are a form of saturation nonlinearity that causes distortion in the unit impulse responses.

RC Fixed, Modulation Depth Variable

Fig. 6 shows the analog voltage outputs (left column) and pulse rates (right column) of outputs *A* and *P*, respectively, that resulted from an input test signal of four PRBS periods applied to the linear circuit of Fig. 5 *a,b*. The filter time constant was fixed at RC = 0.241 s. The rectangular bins in the left column represent the analog voltage outputs as averaged over each state of the PRBS; whereas the bins in the right column represent the number of pulses that occurred during each PRBS state. The modulation depth, as defined in the legend of Fig. 4, was varied from 100% (Fig. 6 *a,e*) to 400% (Fig. 6 *d,h*), and the analog output amplitudes are seen to be linearly proportional to the modulation depth as expected from a linear circuit. It was of interest, however, to simulate the complete neural inhibition that can be evoked in certain phasic sensory afferents in response to stimulus magnitudes above that which results in 100% modulation of the spontaneous (or carrier) rate. This inhibition can be considered a saturation nonlinearity (or "clipping") that is a serious obstacle to a linear, as opposed to a nonlinear, analysis of the response. The bins with zero counts in Fig. 6 *g,h*, resulting from the negative output voltages in Fig. 6 *d,e*, simulate this effect.

In Fig. 7 *a–h* are shown impulse response estimates obtained by cross-correlating the PRBS input over four periods of the outputs of Fig. 6 *a–h*, respectively and applying

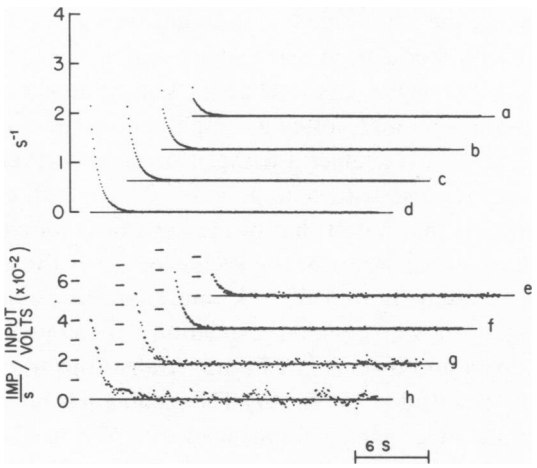

FIGURE 7 Experimental unit impulse response functions (UIRs) of the circuit in Fig. 5 with a fixed time constant $b = 1.5\ s^{-1}$ and variable modulation depth. Four periods of the PRBS input of Fig. 1 were cross-correlated with the linear filter outputs of Fig. 7, and estimates of $h(\tau)$ were computed by the same procedure described in Fig. 6. The modulation depth was varied stepwise: 100% (*a,e*), 200% (*b,f*), 300% (*c,g*), 400% (*d,h*). (*a–d*) Analog voltage UIRs; the relative amplitudes were linearly proportional to the modulation depth except for small displacements of the initial points at $h(0)$. (*e–h*) Pulse interval UIRs; the relative amplitudes were linearly proportional to the modulation depths except for *g* and *h* in which spurious base-line oscillations and restricted amplitudes of the initial displacements at $h(0)$ resulted from the saturation nonlinearities shown in Fig. 7 *g,h*.

the procedure of Fig. 5. The exponential decay portions of Fig. 7 *a–d* agreed to within a good approximation with the theoretical response curve for $b = 1.5\ s^{-1}$ (Fig. 4 *c*) and the amplitudes exhibited an approximately linear relation with the modulation level. The initial points (at $\tau = 0$) of the analog voltage UIRs in Fig. 7 *a,b,* which were corrected for the simulated transducer errors by applying the factors in Eq. 14, have amplitudes that are too large by about 20% relative to those expected from the theoretical plot shown in Fig. 4. In contrast, the amplitude of the initial point of Fig. 7 *c* is in good agreement with that predicted theoretically. This implies that the correction factors in Eq. 14 are more accurate for certain modulation depths than others. These estimates were not digitally smoothed and the 255 points in each plot exhibit scatter along the base line resulting in part from statistical noise inherent in the technique and also from the rectangular averaging used in binning the output data in Fig. 6 *a–d*. The variance of these base-line points would be reduced by averaging over more PRBS periods and/or employing standard digital smoothing techniques. The pulse train impulse responses (Fig. 7 *e–h*) exhibited more point variance than for the analog data; however, the envelopes of points in 7 *e,f* reflected the general contour of the theoretical response. Figs. 7 *g,h* showed spurious oscillations that reflect directly the "clipping" nonlinearity in the outputs of Fig. 6 *g,h*. These oscillations would *not* be reduced by averaging over more PRBS periods and represent a characteristic pattern that is enhanced as the total duration of output clipping is increased. The clipping has the

further effect of reducing the amplitude of the initial response point so that a linear relation of amplitude with modulation depth is not apparent in Fig. 7 *g,h*. The point variance of Fig. 7 *e,f*, which is not due to clipping, can be attributed to three factors. (*i*) The autocorrelation histogram (plotted as amplitude vs. time) of a regularly timed pulse train has a pattern that resembles a damped sinusoid (Perkel et al., 1967). The cross-correlation of white noise with a time series that is autocorrelated has been shown to produce patterns that reflect that of the autocorrelation (Bartlett, 1955). In addition, however, the periodic nature of the PRBS input has the effect that a portion of the autocorrelation pattern is folded back and summed point-by-point with an earlier portion analogous to the "circular correlation" encountered in the frequency domain when using direct and inverse fast Fourier transforms to cross-correlate periodic time series (Gold and Rader, 1969). (*ii*) The rectangular bins used in the histograms of Fig. 6 (*e–h*) introduce higher frequencies than the bandwidth of the PRBS input which results in the occurrence of spurious frequencies in the cross-correlation because of aliasing. This could be minimized by sampling the spike train before the cross-correlation computation with a digital algorithm that does not produce aliased components in the modulation band (French and Holden, 1971). (*iii*) The technique of using PRBS noise stimuli to produce impulse response estimates has an inherent signal-to-noise (S/N) resolution that is a function of the input amplitude, the number of periods applied and the presence of other autocorrelated noise sources (Clarke and

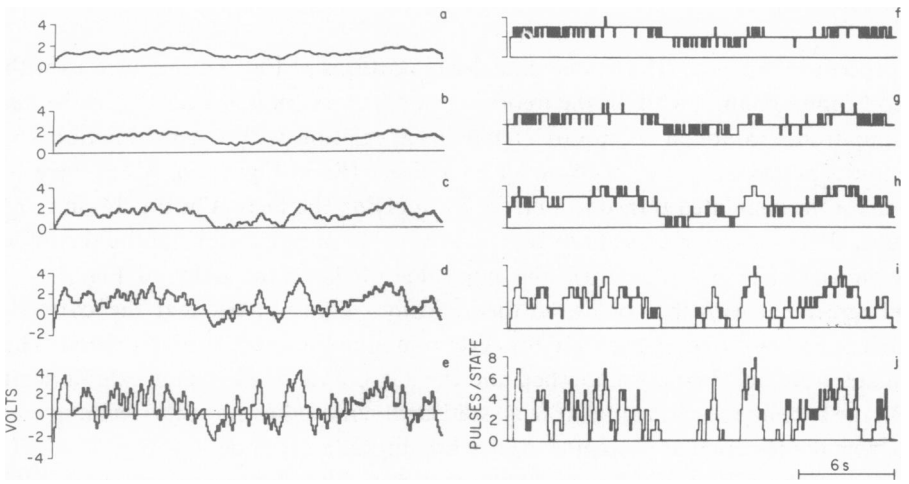

FIGURE 8 Responses of the linear filter circuit of Fig. 5, with a fixed dc modulation depth of 300% but variable time constants, to four periods of the PRBS input of Fig. 1. The scales and units are the same as in Fig. 7. Left column: analog voltage outputs at *A* of Fig. 5 with five different time constants $b = 1/RC\ s^{-1}$ with values: *a* 0.23, *b* 0.33, *c* 0.69, *d* 1.5, and *e* 3.3. Right column: pulse rate modulator outputs corresponding to the analog voltages in the left column. The voltage divider *S* in Fig. 5 *a* was adjusted to produce a spontaneous carrier rate of 40 pulses/s and this carrier was modulated only for positive analog voltages. "Clipping" occurred in *g* and *h* because of the negative analog voltage excursions that resulted from higher frequencies in the filter passbands.

Briggs, 1970; Williams and Clarke, 1968). In general, the S/N of the impulse response estimates can be maximized, and the influences of error sources (*i–iii*) reduced, by using the largest input amplitude that is compatible with the experimental conditions and averaging over at least four periods of the output response before performing the cross-correlation computation.

RC Variable, Modulation Depth Fixed

Results for the protocol RC variable and modulation depth fixed at 300%, are shown for the output responses in Fig. 8 and the impulse response estimates in Fig. 9 resulting from four PRBS periods. The progressive increase in analog output amplitude (Fig. 8 *a–e*) is a direct result of the progressive change in the filter cutoff frequency over the range 0.19–2.6 Hz, respectively. The pulse train outputs in Fig. 8 *i,j* show clipping analogous to that shown in Fig. 6 *g,h*. The impulse response estimates from the analog outputs (Fig. 9 *a–e*) are in excellent agreement with the theoretical values shown in Fig. 4 *c*, except for the aberrant initial point of Fig. 9 *c*. The pulse train impulse response estimates (Fig. 9 *f* to *l*) have point variances and resolutions of the initial peaks that are of the same general range as those observed for semicircular canal afferents as described below.

Impulse Response Estimates from Semicircular Canal First-Order Afferents

Figs. 10 and 11 show impulse response estimates obtained by cross-correlating the spike train outputs from unit first-order semicircular canal afferents with stimuli in the

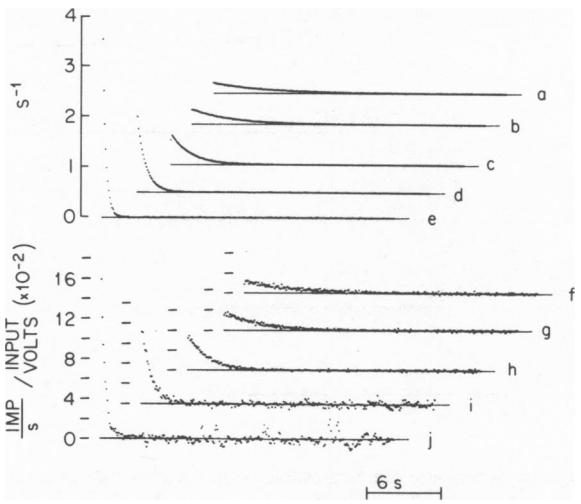

FIGURE 9 Experimental impulse response estimates computed by cross-correlating four periods of the outputs of Fig. 9 with the PRBS input of Fig. 1. (*a–e*) The estimates resulting from the analog outputs in Fig. 9 *a–e*, respectively. (*f–j*) The estimates resulting from the modulated pulse train outputs in Fig. 9 *f–j*, respectively. Theoretical values for these estimates are shown in Fig. 5 *c*. The experimental points were corrected for the bandwidth limitation errors as described in Appendix B. The spurious base-line oscillations in *i* and *j* are the result of the clipping that is shown in Fig. 9 *i,j*.

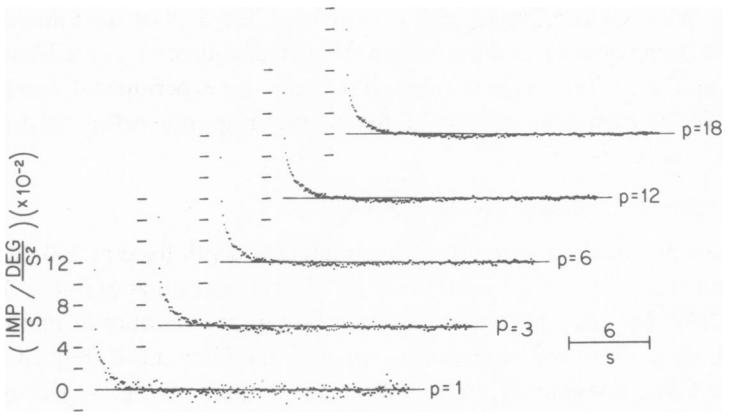

FIGURE 10 Impulse response function estimates of a semicircular canal first-order afferent spike train (unit T20-1), as computed by the procedure summarized in Fig. 6, are shown as a function of the number of periods p of the PRBS. Each point represents the estimate as averaged over successive state durations Δt = 92.0 ms. The point variance decreases approximately as a function of $p^{1/2}$. The estimate for larger values of p shows a resolvable overshoot of the base line. The correction factors for the input transducer errors as computed from Eq. 14 were 1.27 $h(0)$, 1.0 $h(\Delta t)$, and 0.99 $h(n\Delta t)$, $n > 1$, and the corrected values are shown in the figure.

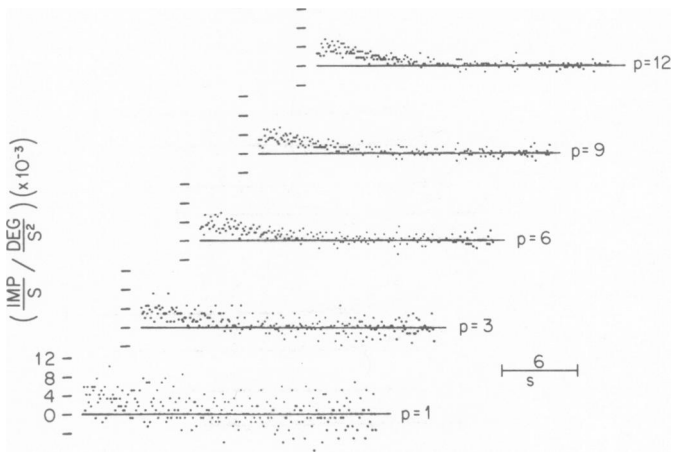

FIGURE 11 (*a–e*) Impulse response function estimates of a semicircular canal first-order afferent (unit H32-6) as averaged over PRBS periods p from 1 to 12. Each point represents the estimate as averaged over the state durations Δt = 92.0 ms. The computations used were identical to those employed for the responses of Fig. 10. The relatively low sensitivity of this unit resulted in magnitudes of $h(\tau)$ points that are scaled an order of magnitude lower on the ordinate than those of Fig. 10. In contrast to the estimates shown in Fig. 10, this unit has an impulse response with a resolvable rising edge toward a maximum followed by a slower decay back toward the base line; the response profile was fit by nonlinear regression to the overdamped second-order exponential linear systems representation $h(\tau) = 0.008 \exp(-0.285\tau) - 0.006 \exp(-1.88\tau)$.

form of the rotational acceleration PRBS input shown in Fig. 1. Each UIR was obtained by applying the stepwise procedure, and the same computer analysis programs, described for the filter circuits (e.g. Fig. 5), however, the number of periods of the output data that were averaged prior to the cross-correlation was varied. The overall resolution of the UIR is seen to increase by averaging over p periods approximately as a function of $p^{1/2}$. In Fig. 10, the point variance for $p \geq 6$ is reduced sufficiently to enable resolution of a slight "overshoot," or negative component, in the UIR. In Fig. 11 the effect of averaging on resolution is particularly striking. A resolvable positive-slope region is evident visually in the early phase of the UIR point envelope for $p \geq 9$, whereas this rise cannot be distinguished clearly in responses for $p \leq 6$. An exponential early rise of the response is characteristic for that of an overdamped second-order linear system.

The magnitudes of peak values of $h(\tau)$ for the unit in Fig. 11 are more than an order-of-magnitude smaller than those of the unit in Fig. 10 as shown by the difference in ordinate scale factors. This is a direct result of the difference in sensitivities of the units as measured by the relative depths of modulation of the spike train responses to the PRBS input.

Determination of Low-Order Linear System Parametric Models of Impulse Responses

In Fig. 12*a* is shown a parametric model of the experimental impulse response shown in Fig. 12*b*. The parametric model is determined from the nonlinear regression fit to the second order exponential series described in the legend. This model has only four parameters, as compared with the 255 points of the experimental impulse response, and the fewer parameters can provide inferences concerning the underlying physiological mechanisms of the receptor transduction process as described in O'Leary and Honrubia (in preparation). But it is necessary to consider the relative validity of both types of models as representations of the system input-output characteristics. Because both of the models in Fig. 12*a,b* are representations based on linear system theory, it is necessary to consider whether the semicircular canal transduction system indeed responded linearly within an acceptable approximation. An excellent test of the validity of a model is to determine whether the model can predict the output to a white noise input which agrees favorably with the system's experimental response (Marmarelis and Naka, 1973*a*). This was tested for the models shown in Fig. 12 by comparing the experimental afferent response with that predicted, by linear convolution with the white noise input, from each of the two model representations. The experimental afferent response to the white noise input is shown in Fig. 12*c*, and the predicted responses from Figs. 12*a* and *b* are shown in Figs. 12*d* and *e*, respectively. The predicted responses are seen to be in relatively good agreement qualitatively with the experimental response, but a conventional quantitative measure of the goodness-of-fit is the magnitude of the percent mean-square-error (%MSE) of the prediction relative to the experimental response. The %MSEs for the parametric and nonparametric impulse

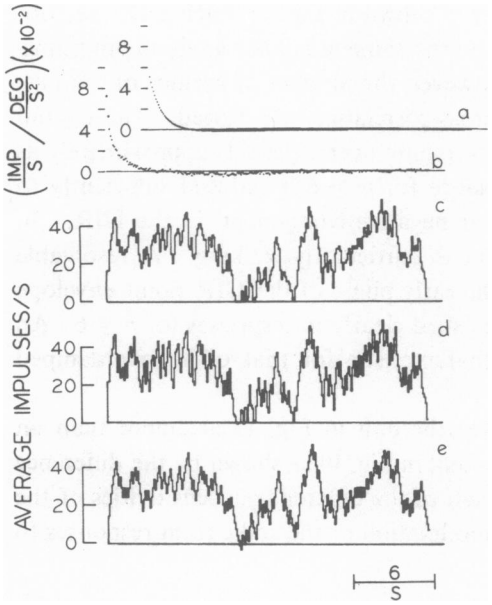

FIGURE 12

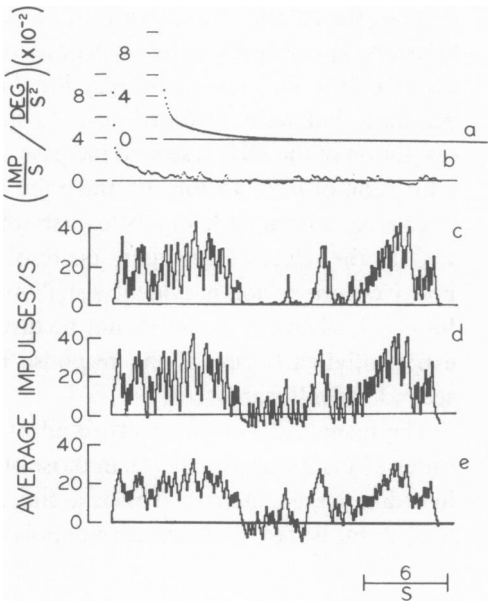

FIGURE 13

FIGURE 12 Parametric and nonparametric impulse response models and their respective linear convolution output predictions to the PRBS input. (*a*) The parametric model is shown plotted from the equation $h(\tau) = 0.057 \exp(-1.11\tau) - 0.003 \exp(-0.047\tau)$ in which the numerical parameters were determined by the nonlinear least squares regression technique described in Methods. The parametric model was fitted from the experimental unit impulse response from unit T20-1 shown in *b*. The latter corresponds to that shown in Fig. 10*f*, but does not include the corrected magnitudes of the input transducer errors. (*c*) The experimental afferent response of this unit as averaged over 10 periods of the PRBS input stimulus. The response profile resembles approximately the rotational stimulus velocity trajectory shown in Fig. 1*d*. (*d*) This profile was predicted by linear convolution from the experimental unit impulse shown in *b*. This prediction is in agreement with the experimental trajectory shown in *c* within a percent mean square error of 7.3%. (*e*) This trajectory was predicted from the parametric linear system model shown in *a*. It is in agreement with the experimental trajectory shown in *c* within a percent mean square error of 8.1%.

FIGURE 13 Parametric and nonparametric impulse response models and convolution predictions plotted according to the format shown in Fig. 12, but for a semicircular canal afferent that exhibited "clipping" of the response trajectory. (*a*) The parametric model is shown plotted from the equation $h(\tau) = 0.021 \exp(-0.351\tau) + 0.028 \exp(-3.23\tau)$. The parameters were determined by a nonlinear least squares regression fit to the experimental unit impulse response shown in *b*. The latter shows spurious oscillations in the base line resulting from nonlinearities resulting from the lack of impulses over the mid-portion of the experimental response trajectory shown in *c*. (*d*) The predicted trajectory is shown resulting from linear convolution of the experimental unit impulse response in *b* with a PRBS input. This prediction shows spurious "negative" activity and is in agreement with the experimental trajectory within a percent mean square error of 8.3%. (*e*) The predicted trajectory is shown as computed by linear convolution of the parametric unit impulse response in *a* with the PRBS input. This prediction is in agreement with the experimental trajectory in *c* within a percent mean square error of 15.7%.

response models were found to be 8.2% and 7.3%, respectively. These values resulting from the linear prediction are significantly less than those resulting from white noise inputs in the visual system (Marmarelis and Naka, 1974). This discrepancy is due in large part to the fact that the semicircular canal unit in Fig. 12 did not exhibit a significant saturation nonlinearity caused by a complete inhibition of firing over a portion of the white noise stimulus, whereas this form of nonlinearity was relatively common in the visual system afferent responses.

It is necessary to consider therefore what %MSE would result from a semicircular canal afferent neuron that did indeed exhibit a clipping nonlinearity over a portion of the white noise stimulus. Fig. 13 *b* shows the experimental impulse response as computed by cross-correlation from the experimental afferent response shown in Fig. 13 *c*. The latter shows complete inhibition from firing over the mid-portion of the stimulus. Fig. 13 *d* shows the predicted response which exhibited a spurious negative activity during that segment of the white noise stimulus in which the experimental response shows a complete inhibition from firing. However, the %MSE of Fig. 13 *d*, relative to that of Fig. 13 *c*, is only 8.3%, which implies that the nonlinear contribution which resulted in the spurious oscillations in the experimental impulse response, had a small effect relative to the linear contribution. The parametric linear model, shown in Fig. 13 *a*, resulted in a prediction with a similar spurious negative-going activity as shown in Fig. 13 *e*. The %MSE for this prediction is 15.1%, which is due in large part to the smoother response contour in the prediction relative to that in the experimental data. The results of Fig. 13 imply that the degree of clipping shown in Fig. 13 *c* did result in a nonlinear contribution, however, this contribution is still significantly less than that observed in the visual system data cited above, and the linear approximations can be considered valid for modeling purposes.

In order to determine whether the relatively accurate linear descriptions described in Figs. 12 and 13 were a general property of afferents from this receptor, the impulse responses of 62 semicircular canal afferent units were computed and linearly convoluted with the white noise input to result in response predictions analogous to those shown in Figs. 12 *d* and 13 *d*. The %MSE of the predicted responses relative to that of the experimental responses were then computed and are shown displayed as a histogram in Fig. 14. The histogram maximum is in the 5–10 %MSE range, and the mean and standard deviation were 10.2 ± 5.9 SD, respectively. We concluded therefore that the small-signal linear analysis provided by the PRBS white noise cross-correlation technique produced nonparametric models in the form of experimental impulse responses which are sufficiently accurate to be used for inferences concerning the underlying physiological transduction mechanisms of the semicircular canal. For example, the striking differences between the impulse response contours of Figs. 10 and 11 imply that a single semicircular canal is innervated by afferents with distinctly *different* linear system response characteristics which cannot all be explained by the simple overdamped pendulum model described classically for this receptor. Moreover, distinct classes of afferent response characteristics were observed in our studies that were correlated with the anatomical regions of innervation of the receptor. These physiological

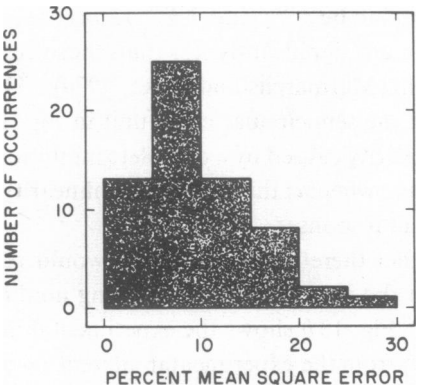

FIGURE 14 Histogram of the percent mean square error (%MSE) of the predicted vs. experimental responses to the PRBS input resulting from a sample of 62 unit impulse responses from afferents innervating the semicircular canal. The mean and standard deviation are 10.2 ± 5.9 %MSE, respectively.

and anatomical descriptions formed the basis for a preliminary report (O'Leary et al., 1974) and are described in detail in a forthcoming publication (O'Leary and Honrubia, in preparation).

DISCUSSION

Physiological investigations of sensory systems have often employed theoretical concepts and analytical techniques from systems and control theory in describing and modeling the systems. In this approach, a substage of the system is considered as a "black box" containing unknown elements to be identified, through analysis of experimentally determined input-output transformations, as corresponding to characteristic systems representations in either the frequency or time domains. A rationale for this approach is that sensory substages can be modeled by equivalent mathematical expressions by the manner in which past inputs are transformed, or filtered, to produce information observable at the present time at the system's outputs. A goal is to obtain equivalent filter representations that can be used to predict, within acceptable resolution limits, the outputs resulting from inputs that span physiological ranges. Subsequent analysis of these representations can suggest insights into underlying physiological processes that operate at the organ, cellular, or membrane levels to determine the cybernetic (communication and control) properties of the systems.

The use of pseudorandom binary noise as an experimental input for the purpose of obtaining models of sensory systems is valuable because it provides data for modeling at two separate levels. First, an on-line estimation of the system performance in the form of a unit impulse response is obtainable immediately for evaluation during the experiment. This initial perspective provides essential information such as the memory of the system, quantitative estimates of sensitivity and the goodness-of-fit of a linear model which can be used to determine an optimum protocol during the experiment.

Second, this approach provides input-output data that can be probed at a deeper level in the form of low-order linear systems models obtained off-line by least-squares fitting of the experimentally determined impulse responses. Moreover, although impulse responses acquired on-line are in the form of time domain linear system descriptions, they can be transformed easily into frequency domain descriptions by employing Fourier transformations; and, in addition, the data can be used to compute nonlinear descriptions in the form of second order Wiener-Volterra integral equations by employing algorithms developed by Ream (1970). The choice of a particular form of the above data descriptions, and a judgement concerning the relative significance of the observed nonlinear influences, should be made with a clear perspective of the goals of the identification analysis.

Finally, it is necessary to emphasize that neither time nor frequency descriptions in themselves can be used to predict a unique linear configuration, such as serial as opposed to parallel, of the components of the system as identified in the analysis (Eykhoff, 1974). For that reason, it is useful to combine a systems identification analysis of the type described in this report with other techniques such as the histological tracing of innervation patterns of a receptor (O'Leary et al., 1974) in order to infer accurately the system's physiology.

APPENDIX A

Pseudorandom Signal Correlation Analysis

Two time-dependent signals $x(t)$ and $y(t)$ are considered correlated if the value of one of them at any time t depends in some way on the value of the other (Lee, 1960). This interdependence is described by the cross-correlation function (CCF) defined as

$$\phi_{xy}(\tau) = \lim_{T\to\infty} \frac{1}{2T} \int_{-T}^{T} x(t)y(t + \tau)\,dt. \tag{16}$$

Because the range of integration in Eq. 16 is over the entire time axis for each fixed time shift (or relative lag) τ between the two signals, $\phi_{xy}(\tau)$ describes the average dependence between two signals separated in time by τ. For the special case $y(t) = x(t)$, Eq. 16 is defined as the autocorrelation function (ACF)

$$\phi_{xx}(\tau) = \lim_{T\to\infty} \frac{1}{2T} \int_{-T}^{T} x(t)x(t + \tau)\,dt, \tag{17}$$

which describes the quantitative dependence of the present value of a signal on past values.

For a system with single input $x(t)$ and single output $y(t)$, the unit impulse response (UIR) can be estimated from the CCF of $x(t)$ and $y(t)$. The convolution integral described in Methods as Eq. 1 can be rewritten as

$$y(t) = \int_{-\infty}^{\infty} h(s)x(t - s)\,ds. \tag{18}$$

The lower limit has been extended to infinity since the UIR must be zero before the input is applied (i.e., an output response cannot occur before an input stimulus). The upper limit has been increased to infinity because the entire UIR, which will decay to zero as t approaches infinity, is included. By substituting Eq. 18 into Eq. 16, the CCF may be rewritten as

$$\phi_{xy}(\tau) = \lim_{T\to\infty} \frac{1}{2T} \int_{-T}^{T} x(t) \int_{-\infty}^{\infty} h(s)x(t + \tau - s)\,ds\,dt, \tag{19}$$

which by interchanging the order of integration becomes

$$\phi_{xy}(\tau) = \int_{-\infty}^{\infty} h(s)\left\{\lim_{T\to\infty} \frac{1}{2T} \int_{-T}^{T} x(t)x(t + \tau - s)\,dt\right\} ds. \tag{20}$$

The term within the brackets is the ACF of the input signal $x(t)$ with an argument $(\tau - s)$ so that

$$\phi_{xy}(\tau) = \int_{-\infty}^{\infty} h(s)\phi_{xx}(\tau - s)\,ds. \tag{21}$$

Eq. 21 can then be solved for $h(s)$ provided that the ACF $\phi_{xx}(\tau)$ of the input signal is either known or computed from Eq. 17 and that $\phi_{xy}(\tau)$ has been computed from Eq. 16. The determination of $h(s)$ for the system from experimentally estimated $x(t)$ and $y(t)$ "identifies" the system in the sense that Eq. 1 can then be used to predict the output which would result from any realizable input. Furthermore, frequency domain transfer function descriptions of the system can be derived from $h(s)$ by computing the Fourier transform

$$F(\omega) = \int_{-\infty}^{\infty} h(\tau)e^{-j\omega\tau}\,d\tau, \tag{22}$$

where $F(\omega)$ is defined as the frequency response function, and then applying the appropriate definitions for gain, phase and coherence spectra (Otnes and Enochsen, 1972).

A white noise input has a particularly simple ACF which leads to an easily determinable solution for $h(s)$ in Eq. 21. By definition, the power density spectrum of white noise is constant over a bandwidth wider than that of the system to be identified, i.e.,

$$\Phi_{xx}(\omega) = 2\pi K, \tag{23}$$

where K is a constant. The ACF can be determined from the Fourier transform of the power-density spectrum by applying the Wiener-Khinchine theorem (Lee, 1960)

$$\phi_{xx}(\tau) = \frac{1}{2\pi} \int_{-\infty}^{\infty} \Phi_{xx}(\omega)e^{j\omega\tau}\,d\omega \tag{24}$$

which for a white noise input becomes

$$\phi_{xx}(\tau) = K \int_{-\infty}^{\infty} e^{j\omega\tau}\,d\omega = K\delta(\tau) \tag{25}$$

where $\delta(\tau)$ is the Dirac δ-function. By a substitution of Eq. 25 into Eq. 21,

$$\phi_{xy}(\tau) = K \int_{-\infty}^{\infty} h(s)\delta(\tau - s)\,ds$$
$$= Kh(\tau). \tag{26}$$

Thus, the CCF of the white noise input with the output is directly proportional to the UIR $h(\tau)$.

In estimating $h(\tau)$ from experimental data, certain advantages result if the white noise input is not random but pseudorandom; i.e., random within a time period $0 \leq t \leq T$, and then repetitive with period T. In that case, the ACF of the pseudorandom input $x(t)$ is

$$\phi_{xx}(\tau) = \frac{1}{T} \int_0^T x(t)x(t + \tau)\,dt, \tag{27}$$

where the integration limits are now finite because of the periodicity. Expressed as an argument of $(\tau - s)$, Eq. 27 is

$$\phi_{xx}(\tau - s) = \frac{1}{T} \int_0^T x(t)x(t + \tau - s)\,dt. \tag{28}$$

The CCF of Eq. 21 can then be written as

$$\phi_{xy}(\tau) = \int_{-\infty}^{\infty} h(s)\left\{\frac{1}{T} \int_0^T x(t)x(t + \tau - s)\,dt\right\}ds, \tag{29}$$

which after changing the order of integration becomes

$$\phi_{xy}(\tau) = \frac{1}{T} \int_0^T x(t)\left\{\int_{-\infty}^{\infty} h(s)x(t + \tau - s)\,ds\right\}dt, \tag{30}$$

or, by substituting Eq. 18,

$$\phi_{xy}(\tau) = \frac{1}{T} \int_0^T x(t)y(t + \tau)\,dt. \tag{31}$$

The CCF may thus be obtained to its full accuracy, i.e. without any statistical estimation errors, by integration over only one period of the pseudorandom input signal. In contrast, the use of a random input and the subsequent integration of Eq. 26 over the finite time the random signal was applied represents only an approximation to the exact CCF as defined over infinite integration limits. Of course, both approaches will result in some error induced by experimental error (noise), even though this would tend to be minimized because of the cross-correlation approach.

If the UIR $h(\tau)$ is assumed to be zero for $t \leq 0$, then Eq. 21 for a periodic input $x(t)$ becomes (Davies, 1970)

$$\phi_{xy}(\tau) = \int_0^T h(s)\phi_{xx}(\tau - s)\,ds + \int_T^{2T} h(s)\phi_{xx}(\tau - s)\,ds$$
$$+ \int_{2T}^{3T} h(s)\phi_{xx}(\tau - s)\,ds + \ldots. \tag{32}$$

Then from Eq. 26

$$\phi_{xy}(\tau) = K[h(\tau) + h(T + \tau) + h(2T + \tau) + \ldots], 0 \leq \tau \leq T, \quad (33)$$

but if $h(\tau)$ decays to zero in a time less than T this reduces to

$$\phi_{xy}(\tau) = Kh(\tau) \quad (34)$$

in agreement with Eq. 26.

APPENDIX B

Input-Transducer Errors in Pseudorandom Binary Noise Experiments

Godfrey and Murgatroyd (1965) derived theoretically the corrections to be applied to the impulse response discrete point estimates as a result of errors in the input transducers. A summary of only their results that apply to transducer errors of the type shown in Fig. 3 will be described.

Effect of Finite Bandwidth of a PRBS Input. Because the autocorrelation function of the input signal is not a perfect delta function in the time domain, the bandwidth of the signal is necessarily limited in the frequency domain. A perfect PRBS has an autocorrelation function of triangular shape and width $2\Delta t$ as shown in Fig. 2 and the bandwidth is of the order of $1/\Delta t$.

The effect of this finite bandwidth can be seen by expanding the impulse response $h(x)$ in a Taylor series about $x = \tau$

$$h(x) = h(\tau) + (x - \tau)h'(\tau) + \frac{(x - \tau)^2}{2!}h''(\tau) + \cdots \quad (35)$$

The convolution integral reduces to Eq. 1 only to a first-order approximation, and the magnitudes of higher-order derivative terms provide an indication of the accuracy that may be obtained for any given impulse response and PRBS input. As derived by Godfrey and Murgatroyd (1965), the error terms are approximately

$$\frac{1}{12}(\Delta t)^2 h''(\tau), \quad \tau \geq \Delta t \quad \text{and} \quad \frac{1}{3}\Delta t\, h'(0), \quad \tau = 0.$$

These authors noted that if the system has as its fastest transient a term $h(\tau) = ke^{-b\tau}$, where b and k are constants, the error terms are of magnitude $1/12(\Delta t)^2 b^2 h(\tau)$ for $\tau \geq \Delta t$ and $-1/3\Delta t b h(0)$ for $\tau = 0$. In the present application, the percentage errors expressed as fractions of the required term in Eq. 13 for $\Delta t = 0.092$ s and $b = 1.0\ s^{-1}$ are -3.07 and $+0.071\%$ for $\tau = 0$ and $\tau \geq \Delta t$, respectively.

Additional Bandwidth Limitation with Reversible Transition Errors in the Input Signal. Godfrey and Murgatroyd (1965) analyzed the effects of input transducer errors on binary cross-correlation experiments in terms of the transition errors between the binary states. If $i(t)$ produces a signal $j(t)$ in the transducer, the transition error is defined by $e(t) = j(t) - i(t)$. This error will result in subsequent errors in the autocorrelation terms of the PRBS such that

$$\phi_{ij}(\tau) = \phi_{ii}(\tau) + \phi_{ie}(\tau) \quad (36)$$

is the measured value at lag τ, $\phi_{il}(\tau)$ is the theoretical value and $\phi_{ie}(\tau)$ is an additional term resulting from the transition error. A common form of $e(t)$ is a reversible zero-crossing (state transition) error in which a rectangular waveform portion of the ideal PRBS input would be followed in the transducer by a trapezoidal waveform response with symmetrical positive and negative transition slopes. In order to determine $\phi_{ie}(\tau)$ for a reversible $e(t)$, θ was defined as the transition time of the transducer from a $+a$ to $-a$ (or $-a$ to $+a$) PRBS state. Only their results for $\theta \leq \Delta t$, where Δt is the PRBS state duration, will be described since they are relevant to the transducer response described in Fig. 3.

The effect of reversible transition errors is that a second convolution integral occurs in Eq. 21 given by

$$I(\tau) = \int_0^T h(x)\phi_{ie}(\tau - x)\,dx. \tag{37}$$

The error terms which result from $I(\tau)$, which are in addition to the error terms given by Eq. 35, can be determined by a similar Taylor expansion of $h(x)$ about $h(\tau)$.

$$I(\tau) = E_1 h(\tau) + E_2 h'(\tau) + E_3 h''(\tau) + \cdots, \tag{38}$$

where $E_1, E_2, E_3 \ldots$ are constants.

By evaluating the higher-order terms these authors determined the relative errors introduced by the second convolution integral as a function of the magnitude of θ, expressed as a fraction of Δt, and the response characteristics of the transducer. For a transducer that is moved from one binary state to the other by a constant and symmetrically sloped trapezoidal response, the error terms can be expressed as a solution of Godfrey and Murgatroyd's equations 24 by

$$I(\tau) = -\frac{2}{3}\theta\Delta t h'(\tau), \quad \tau \geq \Delta t + \theta \tag{39A}$$

$$I(0) = \frac{1}{2}\theta\left[-\frac{4}{3} + \frac{1}{2}\frac{\theta}{\Delta t}\right]h(0) + \frac{1}{2}\Delta t\left[-\frac{2}{3}\theta + \frac{1}{2}\frac{\theta^2}{\Delta t} - \frac{2}{15}\frac{\theta^3}{\Delta t^2}\right]h'(0), \quad \tau = 0 \tag{39B}$$

$$I(\Delta t) = -\frac{1}{4}\frac{\theta^2}{\Delta t}h(\Delta t) + \frac{1}{2\Delta t}\left[-\frac{4}{3}\Delta t^2\theta + \frac{1}{2}\Delta t\theta^2 + \frac{2}{15}\theta^3\right]h'(\Delta t), \quad \tau = \Delta t. \tag{39C}$$

For a system that has as its fastest transient a term $h(\tau) = ke^{-b\tau}$, where k and b are constants, a substitution of $\Delta t = 0.092$ s, $\theta = \Delta t/5$ and $b = 1\ s^{-1}$ into Eq. 39 results in percentage errors in $h(\tau)$ of -23.6, $+0.130$, and $+1.23\%$ for $\tau = 0$, $\tau = \Delta t$, and $\tau \geq \theta + \Delta t$, respectively. The total percentage error for $h(\tau)$ resulting from *both* the PRBS finite bandwidth and the transducer input error would then be for this example -26.7, 0.200, and 1.30% for $\tau = 0$, $\tau = \Delta t$, and $\tau \geq \Delta t + \theta$, respectively, which implies that only the $h(0)$ term would require a correction that is significant relative to a realistic overall experimental error.

We were aided and encouraged in this study by stimulating discussions with Dr. J. P. Segundo and colleagues and also Doctors D. Strelioff, R. F. Dunn, Clifford Lau, and P. Marmarelis. Warren Kumely and Donald Templin provided innovations in the technical implementation.

This work was supported by National Institutes of Health grants NS09692 and USPHS NS09823-04.

Received for publication 2 December 1974.

REFERENCES

BARTLETT, M. S. 1955. Stochastic Processes. Cambridge University Press, Cambridge.

BIRDSALL, T. G., and M. P. RISTENBATT. 1958. Introduction to linear shift register generated sequences. *U.S.A. Technical Report 90.*

BRIGGS, P. A. N., P. H. HAMMOND, M. T. G. HUGHES, and G. O. PLUMB. 1965. Correlation analysis of process dynamics using pseudo-random binary test perturbations. *Proc. Inst. Mech. Eng.* **179**:37.

CLARKE, D. W., and P. A. N. BRIGGS. 1970. Errors in weighting sequence estimation. II. The effects of autocorrelated noise. *Int. J. Control.* **11**, No. 1:57.

COOLEY, J. W., and J. W. TUKEY. 1965. An algorithm for the machine calculation of complex fourier series. *Math. Comput.* **19**:297.

DAVIES, W. D. T. 1970. System Identification for Self-Adaptive Control, Wiley-Interscience, New York.

DIXON, W. J., ed. 1973. BMD07R nonlinear least squares. *In* BMD Biomedical Computer Programs. University of California Press, Los Angeles. 387.

EYKHOFF, P. 1974. System Identification. John Wiley, New York.

FERNANDEZ, C., and J. M. GOLDBERG. 1971. Physiology of peripheral neurons innervating semicircular canals of the squirrel monkey. II. Response to sinusoidal stimulation and dynamics of peripheral vestibular system. *J. Neurophysiol.* **34**:661.

FLOCK, A. 1971. Sensory Transduction in Hair Cells. *In* Handbook of Sensory Physiology. W. R. Loewenstein, ed. Springer-Verlag, New York. **1**:396.

FRENCH, A. S., and A. V. HOLDEN. 1971. Alias-free sampling of neuronal spike trains. *Kybernetik.* **8**:165.

FUORTES, M. G. F. 1971. Generation of Responses in Receptor. *In* Handbook of Sensory Physiology, Principles of Receptor Physiology. W. R. Loewenstein (Ed.) Springer-Verlag, New York. **1**:243.

GODFREY, K. R., and W. MURGATROYD. 1965. Input-transducer errors in binary crosscorrelation experiments. *Proc. IEEE.* **112**:565.

GOLD, A., and G. RADER. 1969. Processing of Digital Signals. McGraw-Hill, Inc., New York.

GROEN, J. J., O. LOWENSTEIN, and A. J. H. VENDRIK. 1952. The mechanical analysis of the responses from the end-organs of the horizontal semicircular canal in the isolated elasmobranch labyrinth. *J. Physiol. (Lond.).* **117**:329.

KOLMOGOROV, A. N. 1941. Interpolation and extrapolation of stationary random sequences. *Bull. Moscow Univ.*, USSR, Ser. Math. **5**.

LEE, Y. W. 1960. Statistical Theory of Communication. John Wiley & Sons, Inc., New York.

MARMARELIS, P. Z., and K. NAKA. 1973 *a*. Nonlinear analysis and synthesis of receptive-field responses in the catfish retina. I. Horizontal cell ganglion cell chain. *J. Neurophysiol.* **36**:605.

MARMARELIS, P. Z., and K. NAKA. 1973 *b*. Nonlinear analysis and synthesis of receptive-field responses in the catfish retina. II. One-input white-noise analysis. *J. Neurophysiol.* **36**:619.

MARMARELIS, P. Z., and K. NAKA. 1974. Experimental analysis of a neural system: two modeling approaches. *Kybernetik.* **15**:11.

MILSUM, J. H., and G. M. JONES. 1969. Dynamic asymmetry in neural components of the vestibular system. *Ann. N.Y. Acad. Sci.* **156**:851.

O'LEARY, D. P., R. DUNN, and V. HONRUBIA. 1974. Functional and anatomical correlation of afferent responses from the isolated semicircular canal. *Nature (Lond.).* **251**:225.

OTNES, R. K., and L. ENOCHSEN. 1972. Digital Time Series Analysis. Holden-Day, San Francisco, Calif.

PERKEL, D. H., G. L. GERSTEIN, and G. P. MOORE. 1967. Neuronal spike trains and stochastic point processes. I. The single spike train. *Biophys. J.* **7**:391.

PRECHT, W., R. LLINAS, and M. CLARKE. 1971. Physiological responses of frog vestibular fibers to horizontal angular rotation. *Exp. Brain Res.* **13**:378.

REAM, N. 1970. Nonlinear identification using inverse-repeat *m* sequences. *Proc. IEEE.* **117**, No. 1:213.

WIENER, N. 1958. Nonlinear Problems in Random Theory. M.I.T. Press, Cambridge, Mass.

WILLIAMS, B. J., and D. W. CLARKE. 1968. Plant modelling from p.r.b.s. experiments. *Control.* **12**:856.